A DNS evaluation of mixing models for transported PDF modelling of turbulent nonpremixed flames

Alex Krisman[a,*], Joshua C.K. Tang[a], Evatt R. Hawkes[a,b], David O. Lignell[c], Jacqueline H. Chen[d]

[a]*School of Mechanical and Manufacturing Engineering, The University of New South Wales, Sydney, NSW 2052, Australia*
[b]*School of Photovoltaic and Renewable Energy Engineering, The University of New South Wales, Sydney, NSW 2052, Australia*
[c]*Chemical Engineering Department, 350 CB, Brigham Young University, Provo, UT 84602, United States*
[d]*Combustion Research Facility, Sandia National Laboratories, Livermore, CA 96551-0969, USA*

Abstract

Transported probability density function (TPDF) methods are well suited to modelling turbulent, reacting, variable density flows. One of the main challenges to the successful deployment of TPDF methods is accurately modelling the unclosed molecular mixing term. This study examines three of the most widely used mixing models: the Interaction by Exchange with the Mean (IEM), Modified Curl (MC) and Euclidean Minimum Spanning Tree (EMST) models. Direct numerical simulation (DNS) data-sets were used to provide both initial conditions and inputs needed over the course of the runs, including the mean flow velocities, mixing frequency, and the turbulent diffusion coefficient. The same chemical mechanism and thermodynamic properties were used, allowing the study to focus on the mixing model. The simulation scenario was a one-dimensional, non-premixed, turbulent jet flame burning either a syngas or ethylene fuel stream that featured extinction and reignition. This test scenario was selected because extinction and reignition phenomena are sensitive to the mixing model. Three DNS cases were considered for both the syngas and ethylene cases with a parametric variation of Reynolds and Damköhler numbers, respectively. Extinction events became more prevalent with increasing Reynolds number in the syngas cases and with decreasing Damköhler number in the ethylene cases. The model was first tested with the mixing frequency defined from the dissipation rate and variance of mixture fraction. With this definition, for the syngas cases this study finds that the TPDF method is successful at

1

predicting flame extinction and reignition using all three mixing models for the relatively lower and intermediate Reynolds number cases, but that all models under-predict reignition in the relatively higher Reynolds number case. In the ethylene fuelled cases, only the EMST mixing model correctly predicts the reignition event for the two higher Damköhler number cases, however, in the lowest Damköhler number case the EMST model over-predicts reignition and the IEM and MC models under-predict it. Mixing frequency was then modelled based on the turbulence frequency and a model constant C_ϕ, the ratio of scalar to mechanical mixing rates. The DNS cases were reexamined with this definition and the results suggested that the optimal value for C_ϕ is mixing model and case dependent. In particular, it was found in the ethylene case considered that reignition could be achieved with the IEM and MC models by adjusting the value of C_ϕ.

Keywords:

transported probability density function, nonpremixed, ethylene, syngas, mixing, DNS, particle method

1. Introduction

Non-premixed turbulent flames are the predominant combustion mode in aero gas turbine engines, diesel engines, industrial burners and fires. At the mixing rates encountered in practical operation, these flames are challenging to model due to their strong turbulence chemistry interactions.

Transported probability density function (TPDF) methods [1, 2] provide a computationally tractable approach to modelling nonpremixed turbulent flames [3, 4]. In TPDF methods, single point statistics of flow and thermochemical state variables are evaluated using transport equations for their joint probability density functions. This approach has the important advantage that the nonlinear chemical source term appears in closed form [1].

*Mob.: +61 431 912 920, Tel.:+61 2 9385 6196

Email address: `a.krisman@unsw.edu.au` (Alex Krisman)

The so-called composition transported probability density function approach (C-TPDF) has received the most attention to date due its relatively simple implementation in conventional computational fluid dynamics solvers [1, 4]. In this approach, the joint PDF of chemical species composition and an energy variable, such as enthalpy, is evolved, requiring the following components:

- a model for the unclosed molecular mixing term, which requires input mixing frequency;

- a model for turbulent flow, for example a $k-\epsilon$ model or a large-eddy simulation model, providing the modelled mixing frequency, turbulent diffusion coefficient, and mean or filtered velocities;

- physical models for the thermodynamic properties and chemical reaction rates;

- boundary and initial conditions; and

- numerical algorithms to implement the modelling.

The main closure challenge is to develop an accurate model of molecular mixing [5, 6]. A number of mixing models have been proposed. Some of the more frequently considered include the Interaction by Exchange with the Mean (IEM) [7], Modified Curl (MC) [8, 9], and the Euclidean Minimum Spanning Tree (EMST) models [10]. However, the existing literature does not clearly identify the optimal choice of a mixing model. Studies of *experimental* flames performed with the IEM [11, 12, 13], MC [14, 15, 16], and EMST [17, 18, 19] models have all obtained good agreement for experimental results. There are three points which make comparing and evaluating these studies difficult:

- There is uncertainty in the accuracy of the chemical kinetic and other physical models, and they are not frequently the same between studies.

- There is uncertainty in the accuracy of the turbulence modelling, and different choices are made in different studies for the turbulence closure: for example, velocity-composition TPDF, $k - \epsilon$, or LES may be used.

- Numerical parameters such as grid sizes, time-steps, tolerances, and number of particles are practically limited by computational expense, and therefore might not always be sufficient. In addition, the choices made vary between studies.

- Experimental measurements have associated uncertainties and it is not always clear exactly what should be compared between models and experiments.

- The model constant C_ϕ which measures the ratio of turbulent to scalar time scales may be selected arbitrarily to give the best results [20].

- The target flame may vary between studies. Flames with higher levels of extinction and reignition are more difficult targets than more stable flames.

Using direct numerical simulations (DNS) as a numerical experiment against which to compare models has advantages which can help overcome some of these difficulties. For example, a previous study by Mitarai *et al.* [6] compared C-TPDF results with DNS modelling decaying, isotropic, turbulence with a simple one-step chemistry model. The DNS provided the time varying mixing frequency, removing an element of modelling. It was found that the EMST model had the best performance in the mean, however the conditional statistics were inaccurate. A more recent study by Yang *et al.* [21] considered an LES-PDF model of a temporally evolving syngas flame (the same as that considered here). In this study, the DNS provided only the validation data-set– the turbulence modelling was provided by the LES.

In the present study, the C-TPDF approach is considered in a Reynolds-averaged context. Two DNS databases focused on extinction and re-ignition processes in nonpremixed temporally evolving plane jet flames are considered: a set of syngas cases from Hawkes *et al.* [22, 23] (previously modelled with LES-PDF methods [21], LES-linear eddy model [24], and one-dimensional turbulence [25]), and a set of ethylene cases from Lignell *et al.* [26] (previously modelled with one-dimensional turbulence [27]). In contrast to the previous study [21], the mean velocity, turbulent diffusion coefficient, and mixing frequency are taken directly from the DNS. The same models of kinetic rates and thermodynamic properties are

used. These choices eliminate potential sources of modelling error.

The difference between the syngas and ethylene cases are the fuel composition and parametric sweep performed. In the syngas DNS, the Reynolds number was adjusted by changing the jet height and velocity, keeping Damköhler number fixed. In the ethylene DNS, the Damköhler number was adjusted at fixed Reynolds number by altering the dilution of the fuel and oxidant streams to change the chemical time-scales while preserving the location of the stoichiometric mixture fraction relative to the shear layer.

Three cases from each DNS study are considered. From the syngas DNS these are the: Lower (L), Moderate (M), and Higher (H) Reynolds number cases. From the ethylene DNS these are the Higher (1), Moderate (2), and Lower (3) Damköhler number cases. By design, the ethylene cases have similar parameters to the syngas case M, with case 3 most similar to case M. The Damköhler number is sufficiently low in all cases to cause local extinction. Local extinction increases with either increasing Reynolds number in the syngas cases or decreasing Damköhler number in the ethylene cases, due to increasing rates of turbulent mixing relative to the chemical timescales. All cases exhibit reignition later in the simulations as mixing rates relax.

Local extinction and reignition are challenging phenomena to model. Close to the point of extinction or reignition, small changes in mixing rates can cause large changes in the thermochemical state. Thus, results are sensitive to the mixing model. The parametric variation of turbulence levels and fuel type performed in this study provides a graded test for evaluating mixing model performance.

Parametric studies are also performed for the mixing constant, $C_\phi = \tau/\tau_\phi$, which is a measure of the ratio of turbulent to scalar mixing time-scales. Most TPDF modelling has been performed without access to a DNS data-set, in which case a value for C_ϕ must be selected as a model-constant. Since a wide range of values for C_ϕ are quoted in the literature [1, 5, 28, 29, 30], it is worthwhile to conduct a parametric study of C_ϕ against the benchmark of the exact values of a passive scalar mixing frequency extracted directly from the DNS without modelling.

2. Simulation scenario

Both the syngas and ethylene DNS simulated a temporally evolving plane-jet flame. The simulations are completely described in Refs. [22, 26] so only a brief summary is provided here for orientation of the reader. The DNS were initialised with a three-dimensional planar slab of fuel moving in a direction opposite to that of surrounding oxidiser streams on each side. A small turbulent velocity fluctuation was imposed at the initial time which triggered the intrinsic instabilities in the shear layer between the fuel and oxidizer, and the subsequent transition of the plane-jet into a turbulent flame. The flame was initialised from a steady flamelet at the initial time. However, the Damköhler number was sufficiently low so as to cause local extinction, and subsequently, as mixing rates relaxed, reignition occurred. The configuration of the DNS is depicted in Fig. 1.

The three syngas DNS cases (L, M, H) and three ethylene DNS cases (1, 2, 3) represent increasing levels of extinction and reduced reignition due to enhanced turbulent mixing relative to the chemical time-scales.

The configuration permits the formation of a statistical ensemble by averaging in the stream-wise and spanwise directions and using symmetry in the transverse direction, $\hat{\mathbf{y}}$, leaving only a statistical dependence on $\hat{\mathbf{y}}$ and time, $\hat{\mathbf{t}}$. The ensemble average is performed on a mass (Favre) basis, where the Favre-average of property ψ, denoted $\widetilde{\psi}$, is defined as $\widetilde{\psi} = \overline{\rho\psi}/\overline{\rho}$, where the over-line represents a Reynolds-averaged quantity.

The TPDF model is based on a RANS formulation and the turbulence closure is provided directly from the Favre-averaged DNS data. The computational domain is temporally evolving and spatially one-dimensional. The lower boundary corresponds to the centre of the fuel stream and the plane of statistical symmetry in the DNS simulation. The upper boundary corresponds to the outflow from the domain. As there are no initial composition fluctuations, the TPDF simulation is initialised with Favre-averaged thermochemical, turbulence, and mean flow information from the DNS [22, 26].
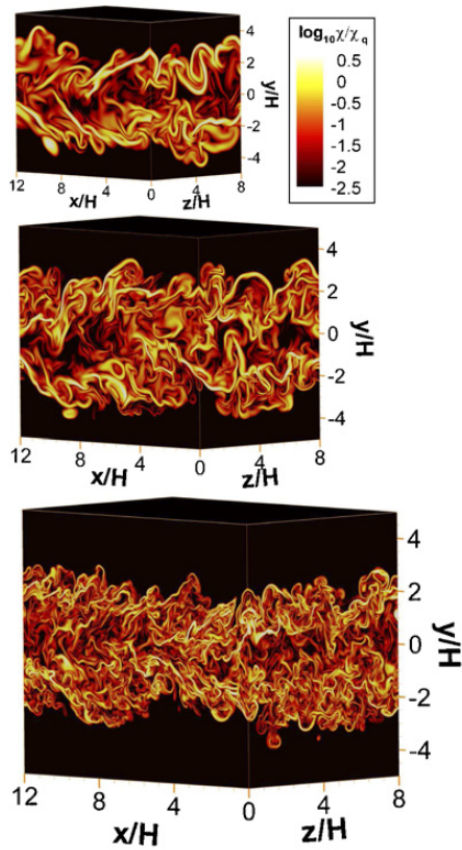
Figure 1: Configuration of the DNS domain, in the syngas case. The domain is coloured by $log\left(\chi/\chi_q\right)$ and shows increasing levels of turbulence from case L (top) to case M (middle) to case H (bottom). The ethylene DNS was performed in an analogous configuration. Image reproduced from Ref. [22].

3. Solution method

The C-TPDF method was implemented using a hybrid particle-mesh approach. An Eulerian mesh is populated with notional Lagrangian particles for which stochastic differential equations are solved. These particles are allowed to undergo chemical reaction, transport in physical space, and mixing with other particles within the same cell. The Eulerian mesh provides cells which are used to calculate local averages of flow properties and bound groups of particles into distinct mixing groups.

The C-TPDF approach usually requires a turbulence closure such as a $k - \epsilon$ model, but this is avoided in the present study by extracting flow information directly from the DNS. The DNS data-set provides turbulence, mean flow, and mixing rate information for the entire computational domain.

Equation 1 is the governing equation for the C-TPDF method [1]. Here $\tilde{f}_\phi$ represents the Favre-joint composition probability density function, V_j are the velocity components, ψ_k are the sample-space species mass fractions, S_k are the production terms for each species, and J_j^k is the scalar flux tensor for species k in direction j.

$$
\begin{aligned}
&\frac{\partial}{\partial t}\left[\langle\rho\rangle\,\tilde{f}_\phi\right] + \frac{\partial}{\partial x_j}\left[\langle\rho\rangle\,\langle V_j|\psi_k\rangle\,\tilde{f}_\phi\right] \\
&+ \langle\rho\rangle\,\frac{\partial}{\partial\psi_k}\left[S_k\tilde{f}_\phi\right] = \\
&\frac{\partial}{\partial\psi_k}\left[\left\langle\rho^{-1}\frac{\partial J_j^k}{\partial x_j}|\psi_k\right\rangle\langle\rho\rangle\,\tilde{f}_\phi\right]
\end{aligned}
\tag{1}
$$

The first two terms on the left hand side of Eq. 1 represent the material derivative of the joint compositional PDF and the third term represents transport in compositional space due to chemical reaction, which is closed. The term on the right hand side represents unclosed molecular diffusion. The conditional expectation of transportation in physical space due to advection, $\frac{\partial}{\partial x_j}\left[\langle\rho\rangle\,\langle V_j|\psi_k\rangle\,\tilde{f}_\phi\right]$, may be approximated using the gradient diffusion hypothesis [31].

The molecular diffusion term has been modelled by various deterministic and stochastic processes, three of which are evaluated in the present study: the Interaction by Exchange

with the Mean [7, 32], Modified Curl's [8, 9], and Euclidean Minimum Spanning Tree [33, 10] models.

The governing C-TPDF equation may be reduced to a set of stochastic differential equations which separately solve for transport in physical and compositional space, as follows:

$$dx(t) = \left[\widetilde{V} + \frac{\nabla \widetilde{\Gamma_T \bar{\rho}}}{\bar{\rho}} \right] dt + \sqrt{2 \widetilde{\Gamma_T}} dW, \tag{2}$$

$$d\phi(t) = [M]dt + [R]dt. \tag{3}$$

Equation 2 represents the transport of particles in physical space. There is a deterministic part, $\left[\widetilde{V} + \frac{\nabla \widetilde{\Gamma_T \bar{\rho}}}{\bar{\rho}} \right] dt$, and a stochastic part, $\sqrt{2 \widetilde{\Gamma_T}} dW$. The deterministic part represents the effects of the mean velocity field and turbulent diffusion. The stochastic part is a Wiener process that models turbulent transport as a random walk with step-size proportional to the square root of turbulent diffusivity and the normal random variable W.[34].

Equation 3 represents the transport in composition space. The first term characterises molecular mixing and this is the focus of the study. The second term is the closed chemical source term which is treated here by solving a system of ordinary differential equations using a 6-stage, 4th order Runge-Kutta numerical method [35]. The equations are supplemented with the thermodynamic equation of state and the ideal gas law.

Equations 2 and 3 represent three distinct, yet coupled, phenomena: transport in physical space (advection), molecular mixing, and chemical reaction. In order to evaluate the model equations a splitting scheme is required to subdivide each time step into partial time steps over which each event is independently evaluated. Strang splitting [36] is used here to solve Eqns. 2 and 3. The particular scheme is a symmetric splitting scheme denoted **TM-RMT** [34, 37]. **T** is transport in physical space, **M** is molecular mixing and **R** is chemical reaction. Transport and mixing are evaluated twice for each iteration and reaction once in a symmetrical manner. The use of a symmetric splitting scheme reduces the splitting discretisation error [37] and provides second order accuracy for the splitting scheme [34]. The evaluation of the **T** sub-step allowed particles to be transported in physical space within a cell, or between adjacent cells. The **M** sub-step was evaluated in each cell with a particular

9

number of particles participating in the mixing event. The **R** sub-step was evaluated for each individual particle.

In order to solve the transport sub-step, **T**, the turbulent diffusivity, $\widetilde{\Gamma}_t$, was required. In order to solve the modelled mixing sub-step, **M**, the mixing frequency, Ω_ϕ, was required. In general, it is possible that different species could experience different rates of mixing [22]. However, this effect is not typically incorporated into models so that in the present work, a non-reacting scalar was used to define the mixing frequency. Therefore, for the ethylene case these values were calculated based on the Bilger mixture fraction, Z, while the mixture fraction based on nitrogen was used in the syngas cases (no reactions involving N were considered, and Ref. [22] has shown that the Bilger and nitrogen mixture fractions had very similar mixing timescales.).

The turbulent diffusion coefficient was calculated as $\widetilde{\Gamma}_t = -\left(\frac{\widetilde{\rho v Z} - \overline{\rho}\widetilde{v}\widetilde{Z}}{\overline{\rho}\nabla\widetilde{Z}}\right)$, where v is the velocity and ρ is the density. Near the domain edges, where $\nabla\widetilde{Z}$ approaches zero, a small number equal to one percent of the maximum $\nabla\widetilde{Z}$ value was added to this term to ensure numerical stability.

For the results in sections 4.1-4.4, the mixing frequency, Ω_ϕ, was calculated from the DNS as $\Omega_\phi = \widetilde{\chi_\phi}/\widetilde{\phi''^2}$ where $\widetilde{\phi''^2}$ is the Favre-averaged mixture fraction variance. $\widetilde{\chi_\phi}$ is the Favre-averaged scalar dissipation rate. The approximation $\widetilde{\chi_\phi} = 2D|\widetilde{\nabla Z}|^2$, where D is the mass diffusivity of N_2 in the syngas cases and the thermal diffusivity in the ethylene cases, was found to be sufficiently accurate as judged by the temporal evolution of mixture fraction root mean square profiles. In section 4.5, mixing frequency was calculated from the turbulence frequency. The relevant equations are introduced in that section.

The required input values were obtained from the Favre-averaged DNS data, which was calculated by ensemble averaging in the statistically homogenous directions $\hat{\mathbf{x}}$ and $\hat{\mathbf{z}}$ at every time step. The required input values were subsequently smoothed with a cubic smoothing spline to reduce statistical noise resulting from the finite sampling of the DNS, and then written to a file as a lookup-up table on a very fine mesh. The data written to look-up tables had two to three times higher resolution than the C-TPDF simulation's Eulerian grid. The table data was linearly interpolated in space and time as required to particle locations during

10

the simulations. Figure 2 presents the DNS-extracted input data for $\widetilde{\Gamma}_t$ and Ω_ϕ from syngas case M. The syngas case M results in Fig. 2 are qualitatively similar in all other ethylene and syngas cases.
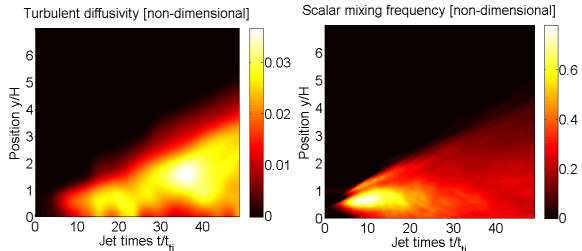
Figure 2: Turbulent diffusivity $\widetilde{\Gamma}_t$ (left), and scalar mixing frequency Ω_ϕ (right) profiles from syngas case M DNS, non-dimensionalised by jet height and jet velocity.

The key numerical parameters in the implementation were the: number of cells, N_{CELL}; number of particles per cell, N_{PC}; and the time step per iteration, t_{step}. A sufficient number of cells was required in order to capture gradients in the fluid domain. The statistical error due to representing the flow by a finite number of discrete particles is of the order $N_{PC}^{-0.5}$ [34]. Unless otherwise stated, all syngas results presented are based on simulations using N_{PC} of 4,000, N_{CELL} of 384, and t_{step} of $5 \times 10^{-8}[s]$, and all ethylene results presented are based on simulations using N_{PC} of 2,000, N_{CELL} of 288, and t_{step} of $1 \times 10^{-8}[s]$. These values were deliberately chosen to be more refined than was actually required in order to rule out numerical error as a reason for the observed differences between the model and DNS.

The IEM, MC, and EMST mixing models considered in this study are well described in the literature and only a cursory summary is provided here for completeness. The mixing term, [M], in Eqn. 3 is evaluated for a given scalar variable, ϕ, of a given particle, i. A brief description of each mixing model follows [6].

- For the IEM model, each particle is mixed with the local mean. The composition of each particle, ϕ_i, evolves is time by:

$$\frac{d\phi_i}{dt} = -\frac{1}{2}\Omega_{\phi,i}\left(\phi_i - \widetilde{\phi}\right),$$

(4)

11

where $\Omega_{\phi,i}$ is the scalar mixing rate interpolated to particle i, ϕ_i is the scalar variable ϕ for particle i, and $\widetilde{\phi}$ is the cell-averaged scalar variable.

- For the MC model, random pairwise mixing is performed. Mixing pairs are randomly selected and their compositions are updated by:

$$\phi_{i,\alpha}(t+dt) = \phi_{i,\alpha}(t) + \frac{1}{2}a\left(\phi_{i,\beta} - \phi_{i,\alpha}\right) \tag{5}$$

$$\phi_{i,\beta}(t+dt) = \phi_{i,\beta}(t) + \frac{1}{2}a\left(\phi_{i,\alpha} - \phi_{i,\beta}\right), \tag{6}$$

where $\phi_{i,\alpha}$ and $\phi_{i,\beta}$ are the compositions of two randomly selected particles, α and β, and a is a uniform random variable on the interval $[0,1]$. The rate at which pairs are selected for mixing is determined by the cell-centered value for the mixing frequency.

- For the EMST model, structured pairwise mixing is performed. Mixing pairs are selected based on their proximity in composition space and their compositions are updated by:

$$\phi_{i,\alpha}(t+dt) = \phi_{i,\alpha}(t) + bB_n\left(\phi_{i,\beta} - \phi_{i,\alpha}\right) \tag{7}$$

$$\phi_{i,\beta}(t+dt) = \phi_{i,\beta}(t) + bB_n\left(\phi_{i,\alpha} - \phi_{i,\beta}\right), \tag{8}$$

where $\phi_{i,\alpha}$ and $\phi_{i,\beta}$ are the compositions of two near-neighbour particles in composition space, b is determined from the mixing frequency, and B_n indicates the proximity of the mixing pair to the centre of the spanning tree in composition space. The EMST mixing model was implemented using the routines available from Ref. [38].

For detailed descriptions and discussions of these models, readers are directed to Refs [4, 6, 7, 32] for IEM, Refs [4, 6, 8, 9] for MC, and Refs [4, 6, 33, 39] for the EMST mixing model. For the present study it is sufficient to outline the key differences between the models:

12

1. All mixing models possess the following properties: mean quantities are conserved, composition values are bounded within physical limits, and variances for all mixed values must decay.

2. The IEM model is deterministic and applied to all particles within the cell at each time step. The MC and EMST models are stochastic and require selection of a mixing-group which is a subset of the particles within a given Eulerian cell.

3. The IEM model mixes each particle with the cell-averaged value. The MC and EMST models conduct mixing on a pair-wise basis. This requires selection of mixing pairs.

4. The role of the mixing frequency in the IEM model is to determine the degree of mixing between each particle and the cell-average based on the particle's local value of mixing frequency. For the MC model, the mixing frequency determines the number of mixing pairs to be selected. For the EMST model, the mixing frequency determines the rate at which particles enter and leave the mixing state, and the rate of mixing.

5. The MC model places no restrictions on which particles may form mixing pairs, apart from preventing a particle from mixing with itself. The EMST model only allows mixing between particles that are near neighbours in compositional space as measured in an Euclidean sense.

6. Due to point 5, only the EMST model has the property of locality in composition space for mixing within a cell. The locality property ensures that only particles of similar composition may mix, and is considered beneficial for an accurate mixing model [10]. As a consequence of having the property of locality in composition space, the EMST model violates the property of independance, and therefore also violates the property of linearity [10]. This shortcoming is rectified by more recent mixing models, such as multiple mapping conditioning [40, 41] and the shadow position mixing model [42].

4. Results and discussion

4.1. Sensitivity to numerical parameters

A sensitivity analysis was conducted for N_{PC}, Fig. 3, and N_{CELL}, Fig. 4.

Fig. 3 shows a converging solution with increasing N_{PC} for the syngas case M. The spatial plots of temperature and mixture fraction at forty-five jet times (after reignition of the jet) collapse to a consistent solution in the large N_{PC} limit. The reason for increasing N_{PC} is to reduce the statistical error which scales as $N_{PC}^{-0.5}$. The use of $4,000$ particles per cell produces a sufficiently smooth solution for cell-averaged information. The large particle number was retained in order to ensure that results were not N_{PC} dependent.
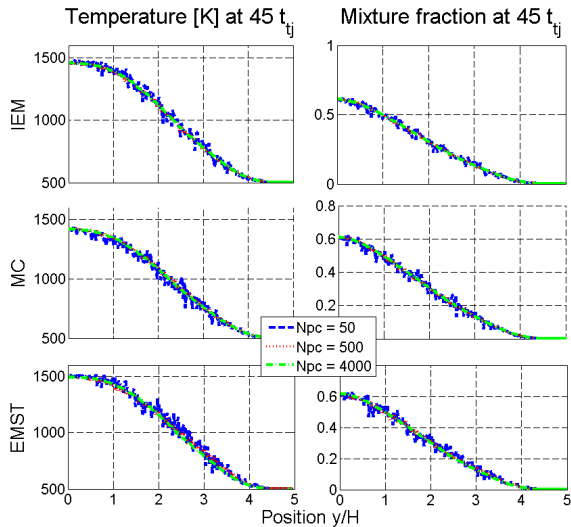
Figure 3: Sensitivity analysis of number of particles per cell, using 384 cells for case M. Temperature (left column) and mixture fraction (right column) are compared at 45 jet times for 50, 500, and 4000 particles per cell. IEM, MC, and EMST all show convergence with increasing N_{pc}.

Fig. 4 shows a converged solution over a large range of N_{CELL}, for the syngas case M. The lack of sensitivity to number of cells is attributed to the availability of flow information from the DNS data set. In most practical situations where a $k - \epsilon$ closure is required it is expected that there would be a greater sensitivity to N_{CELL} and a relatively larger value of N_{CELL} might be required to obtain grid convergence.

The size of the time step was also tested. It was found that the value of 5×10^{-8} [s] in the case of syngas and 1×10^{-8} [s] in the case of ethylene was sufficient.

14
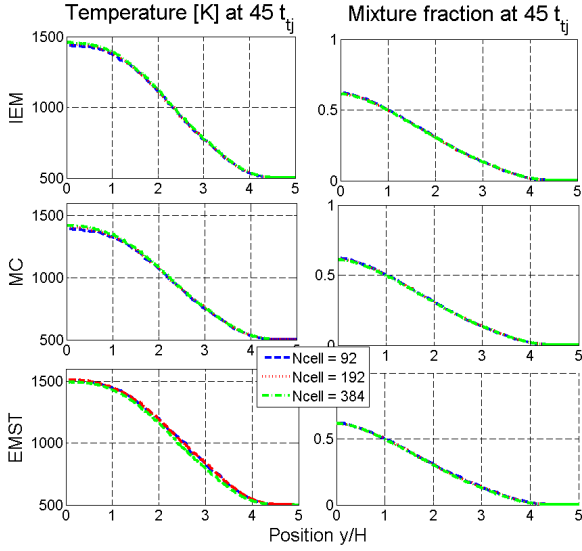
Figure 4: Sensitivity analysis of number of cells, using 4000 particles per cell for case M. Temperature (left column) and mixture fraction (right column) are compared at 45 jet times for 96, 192, and 384 cells. IEM, MC, and EMST all show very similar results for different N_{cell}.

4.2. Mixture fraction

4.2.1. Syngas

Fig. 5 shows the mean mixture fraction versus **y** at $t/t_{tj} = 20$ and 45. The profile is well predicted at both points during the simulation. There is little difference between the mixing models, which is to be expected since the mixing process does not affect the mean of mixture fraction either directly or indirectly through a coupling with chemical reaction. The correct prediction of the mixture fraction profile provides confidence that the flow information extracted from the DNS is being processed correctly and that the numerical implementation of the particle method is consistent.

Fig. 6 shows the spatial profiles of mixture fraction RMS. All mixing models closely predict the DNS values in all cases. There is a small amount of over-prediction early in case L and late in case H. This is probably due to either differential diffusion or to the gradient transport assumption. These results provide confidence that the mixing frequency input from the DNS is being correctly processed and that the mixing models are correctly implemented.

15
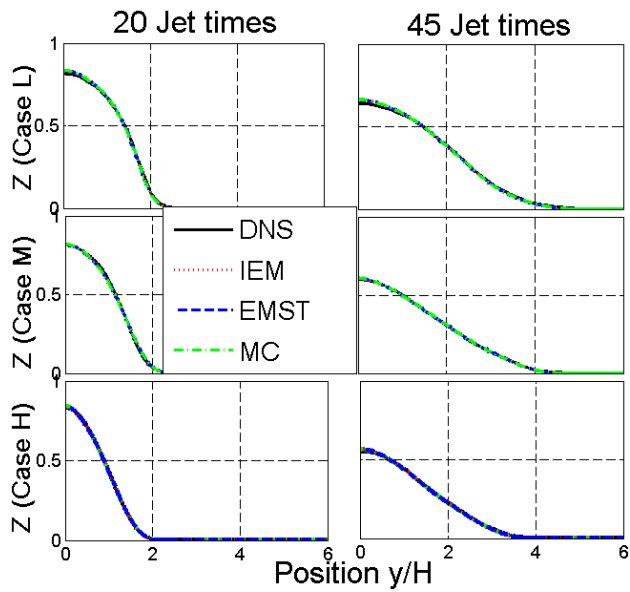
Figure 5: Mean mixture fraction comparison between mixing models and syngas DNS for cases L, M, and H (ordered by increasing Reynolds number and local extinction) at 20 and 45 jet times.
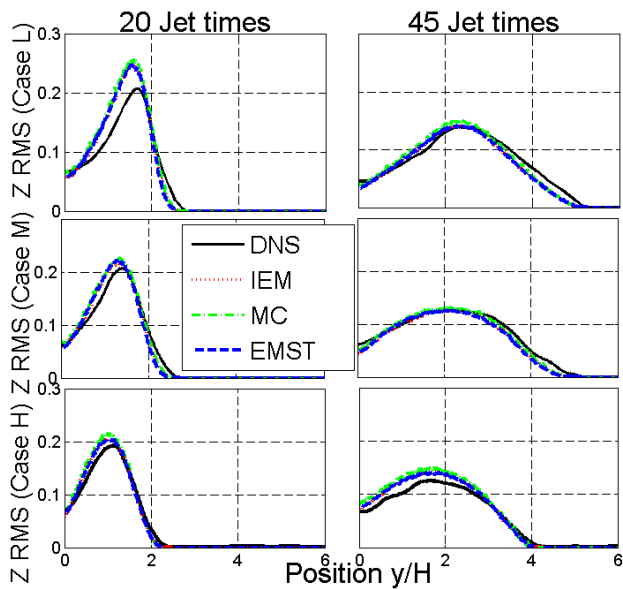
Figure 6: RMS mixture fraction comparison between mixing models and syngas DNS for cases L, M, and H (ordered by increasing Reynolds number and local extinction) at 20 and 45 jet times. All cases closely match the DNS.

16

4.2.2. Ethylene

Fig. 7 presents the mean mixture fraction plots. All mixing models in all cases adequately predict the evolution of mixture fraction.
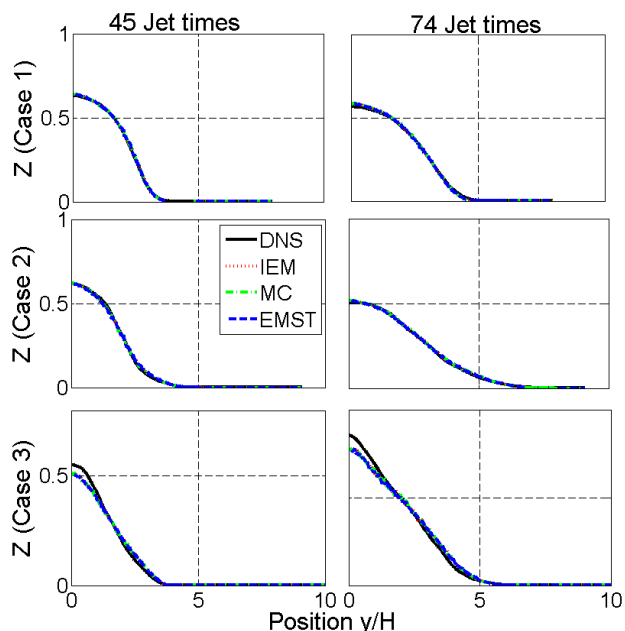
Figure 7: Mean mixture fraction comparison between mixing models and ethylene DNS for cases 1, 2, and 3 (ordered by decreasing Damköhler number and increasing local extinction) at 45 and 74 jet times.

The mixture fraction RMS plots are presented in Fig. 8. All mixing models, in all cases, match the temporal evolution of the mixture fraction RMS to within about 10% of the DNS value.

4.3. Extinction and reignition

4.3.1. Syngas

The most important test is for a qualitatively correct prediction of the extinction and reignition event. Figures 9, 10, and 11 compare the C-TPDF results using different mixing models with the DNS result for increasing Reynolds number and thus levels of extinction. The figures show mean temperature on a colour scale versus normalised time and space.

Case L is well predicted by all mixing models with the correct timing of extinction and reignition simulated. The EMST model does a slightly better job at predicting the
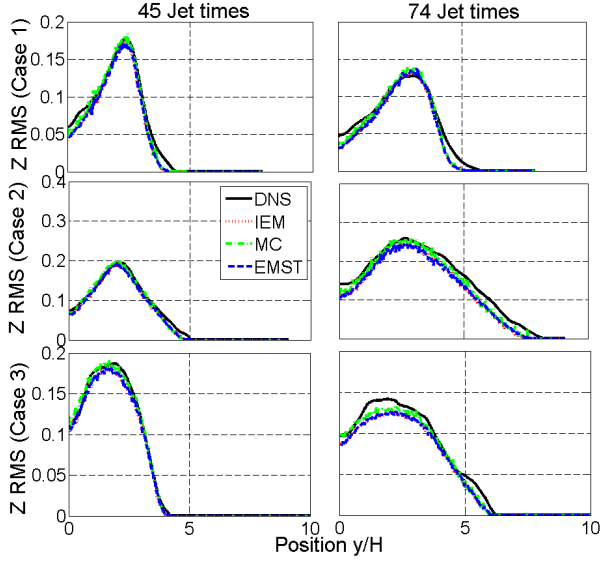
Figure 8: RMS mixture fraction comparison between mixing models and ethylene DNS for cases 1, 2, and 3 (ordered by decreasing Damköhler number and increasing local extinction) at 45 and 74 jet times.

temperature field but otherwise few differences are evident in Fig. 9.

Case M is also well predicted by all mixing models. The higher Reynolds number results in more local extinction in the DNS which is well reproduced by the C-TPDF simulations. Again, the EMST does a slightly better job in reproducing the timing of reignition and the overall temperature field.

As the Reynolds number is pushed even higher in case H the C-TPDF method under predicts reignition. While it is true that all mixing models show signs of reignition occurring, it is significantly delayed compared to the DNS. The EMST model does the best job in predicting the reignition event and the temperature field, with the IEM model slightly worse and the MC model further behind.

Figure 12 presents a quantitative comparison between the DNS and mixing model results for the maximum temperature evolution with respect to time in cases L, M, and H. Significant over prediction of the maximum temperature early in the simulations is observed for all mixing models and in all cases. The EMST model performs the best from 20 jet times onwards, but it performs similarly to the MC and IEM models from 0 to 20 jet times in all cases.

18
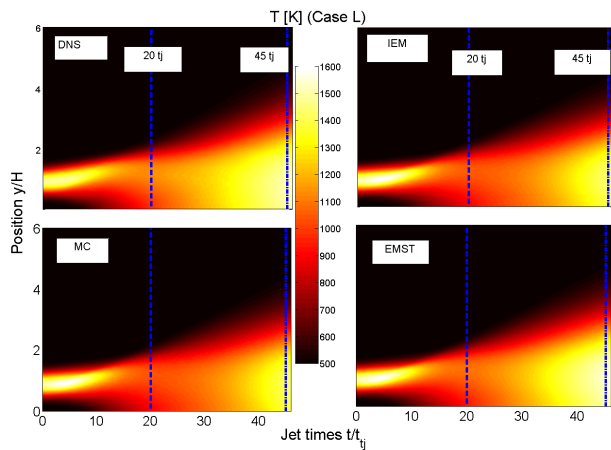
Figure 9: Extinction and reignition for case L. The domain coloured by mean temperature shows the one-dimensional spatial profile's progression over time. The DNS (top left) shows that extinction should occur by 20 jet times and reignition should be well established by 45 jet times.
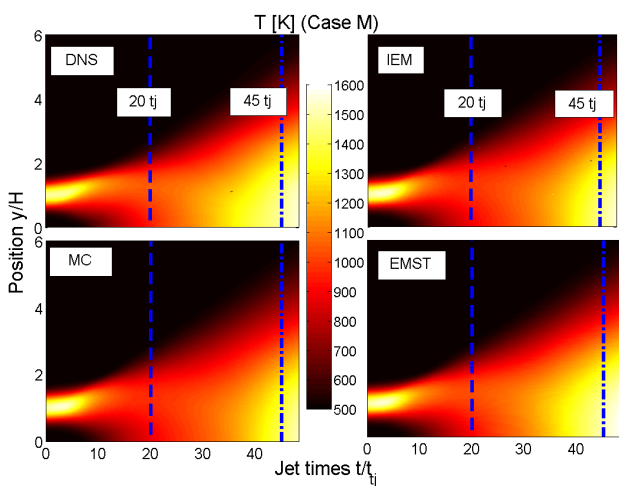
Figure 10: Extinction and reignition for case M. The domain coloured by mean temperature shows the one-dimensional spatial profile's progression over time. The DNS (top left) shows that extinction should occur by 20 jet times and reignition should be established by 45 jet times.
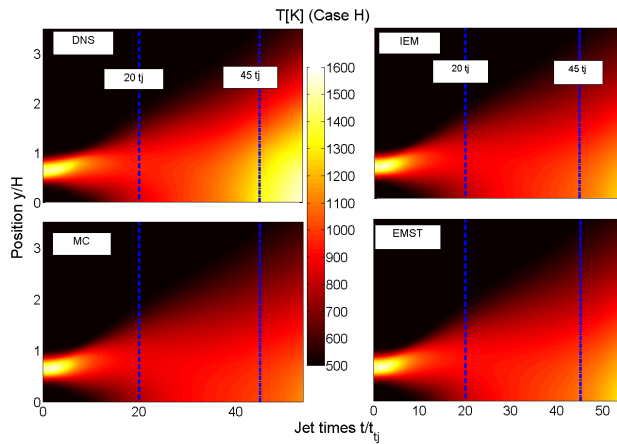
Figure 11: Extinction and reignition for case H. The domain coloured by mean temperature shows the one-dimensional spatial profile's progression over time. The DNS (top left) shows that extinction should occur by 20 jet times and reignition should be well-underway by 45 jet times.
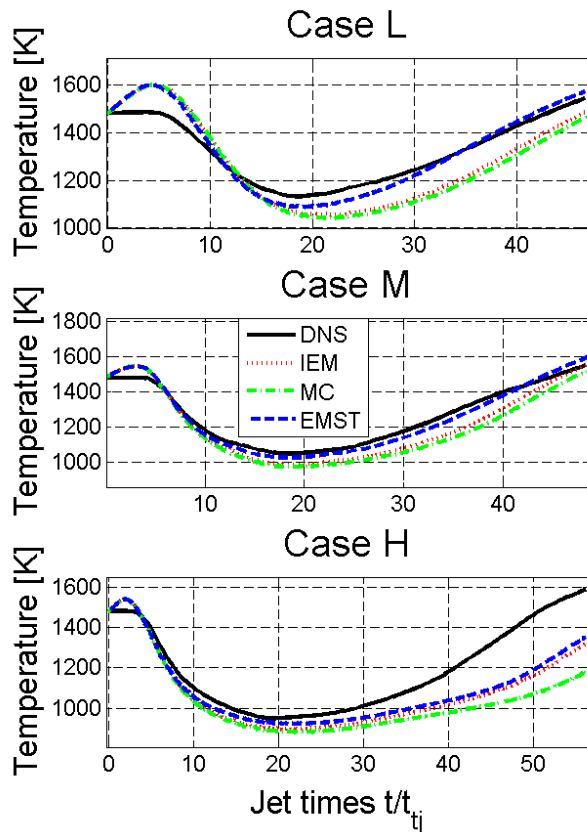
Figure 12: Comparison of maximum mean temperature versus time between mixing models and DNS for syngas cases L, M, and H (ordered by increasing Reynolds number and local extinction).

20

In a previous article involving some of the present authors [22], it was suggested that increased intermittency of the local mixing rate with increased Reynolds number caused the progressively increased levels of extinction going from cases L to M, given that Damköhler number was fixed. It is well known that increased Reynolds number leads to larger fluctuations of scalar dissipation rate relative to the mean [43], which has been argued to cause more extinction [44]. However, the present TPDF modelling does not include intermittency effects, yet it still reproduces the trend of increasing levels of extinction with Reynolds number. Therefore, the present results suggest that intermittency of mixing rate, i.e. mixing rate fluctuations, is not the cause of the increasing levels of extinction with increasing Reynolds number in the present cases. Rather, it suggests that low Reynolds number affects the development of the jet such that *mean* mixing rates are lower in the lower Reynolds number cases, despite having the same large-scale jet timescale. (To further explain this point, the mean mixing rate is well known to be Reynolds-number independent at high Reynolds number, however, at lower Reynolds number molecular effects can become important which acts to reduce the mean mixing rate compared with the high Reynolds number limit.)

Another noteworthy point relating to the present results for case H is that they are inferior to LES-PDF results modelling the same flame presented by Yang, Pope and Chen [21]. In that work, a healthy flame is predicted, in line with the DNS. Here, while the flame is in the process of igniting, it does not fully reignite. This is particularly interesting because the present case is arguably the best that can be done with a RANS-based model, as all of the inputs were taken from the DNS, and yet the results from LES are still superior. This suggests that spatial structure, unresolved by RANS, is important in the process of reignition. Spatially distinct pockets of healthily burning flames may exist and become sources to feed reignition. If such pockets are large-scaled, they would be resolved by LES, which may explain the better predictions of reignition by Ref. [21].

4.3.2. Ethylene

Figures 13, 14, and 15 show the qualitative extinction and reignition behaviour for the ethylene cases 1, 2, and 3, respectively.

21

Case 1, with the largest Damköhler number, has the lowest degree of extinction. As shown in Fig. 13, only the EMST mixing model successfully predicts reignition. The MC and IEM models fail to predict any substantial reignition event, with the MC model performing slightly better than the IEM.

Fig. 14 presents the Case 2 results. Again, only the EMST model predicts the qualitatively correct behaviour. The IEM and MC models appear to perform worse compared to case 1.

The case 3 results shown in Fig. 15 represents the lowest Damköhler number simulation. The levels of extinction are so high that there is no sign of reignition until very late in the simulation (150 jet times compared to 45 jet times in case 2). In the DNS, the prolonged delay in reignition results in thorough mixing and a premixed reignition mode [26]. The IEM and MC models fail to show any signs of reignition. The EMST model, however, predicts far too much reignition and is further from the DNS results in terms of the overall temperature field than the IEM and MC results.
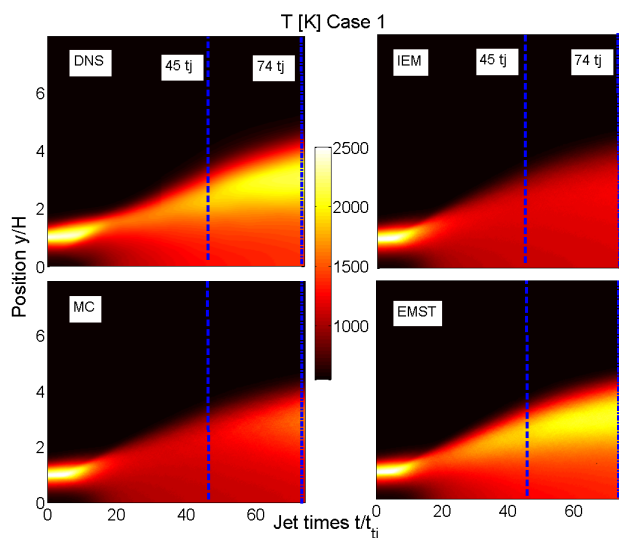
Figure 13: Extinction and reignition for case 1. The domain coloured by mean temperature shows the one-dimensional spatial profile's progression over time. The DNS (top left) shows that extinction should occur by about 25 jet times and reignition should be well-underway by 45 jet times.

Figure 16 shows a quantitative comparison of the evolution of the maximum temperature
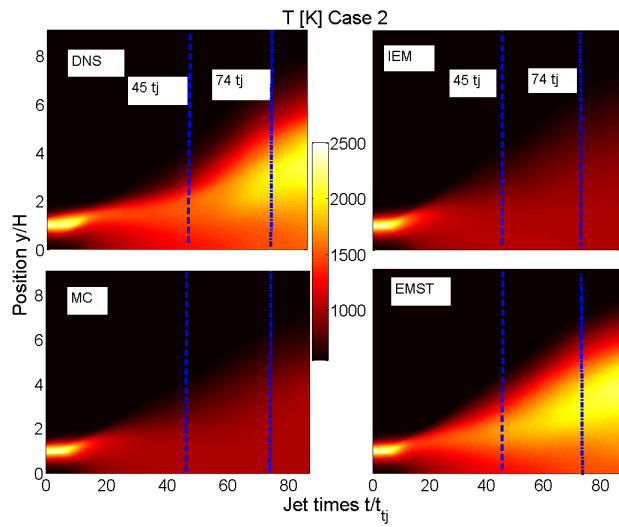
Figure 14: Extinction and reignition for case 2. The domain coloured by mean temperature shows the one-dimensional spatial profile's progression over time. The DNS (top left) shows that extinction should occur by about 25 jet times and reignition should be well-underway by 45 jet times.
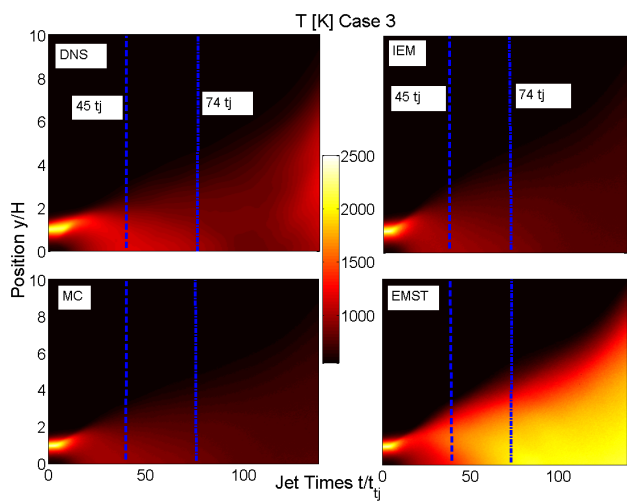
Figure 15: Extinction and reignition for case 3. The domain coloured by mean temperature shows the one-dimensional spatial profile's progression over time. The DNS (top left) shows that extinction should occur by about 25 jet times and reignition should not begin until the end of the simulation, near 140 jet times.

with respect to time between the DNS and mixing models in cases 1, 2, and 3 . All mixing models initially over-predict the maximum temperature in all cases and then are too early in predicting the rapid drop in maximum temperature due to the increasing local extinction. The EMST model has a similar shape in each case and uniformly predicts reignition at about 15-25 jet times, in contrast to the reignition in the DNS, which ranges from about 20-110 jet times. The MC and IEM models are virtually indistinguishable in cases 2 and 3. In case 1, the MC model appears to predict the onset of reignition at a very delayed time, unlike the IEM model.
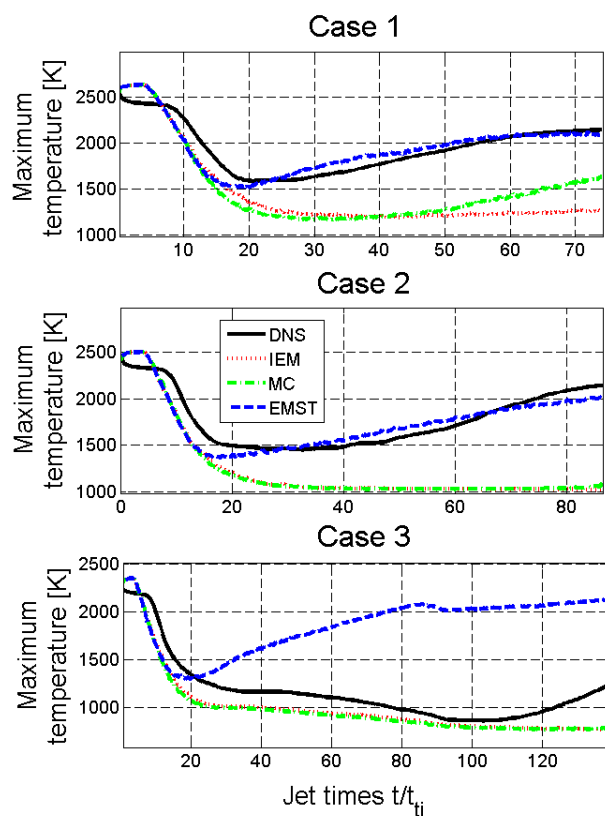
Figure 16: Comparison of maximum mean temperature versus time between mixing models and DNS for ethylene cases 1, 2, and 3 (ordered by decreasing Damköhler number and increasing local extinction).

24

4.4. Conditional profiles

4.4.1. Syngas

Conditional probability density functions were obtained for temperature and OH mass fraction for cases M and H. Cases M and H were selected as they are the best and worst performing of the syngas cases, respectively.

Case M results are shown in figures 17 and 18 for temperature and OH mass fraction, respectively. All mixing models qualitatively predict the conditional mean values quite well, however the EMST model greatly underestimates the conditional variance, or width, of the PDFs.

The results from case H are shown in Figures 19 and 20 for temperature and OH mass fraction respectively. Case H was the most difficult case as it had the highest levels of extinction. This is reflected in the conditional PDFs, which show that all mixing models failed to predict sufficient reignition. The EMST model again fails to correctly predict the variance of the conditional PDFs.

The most striking feature of the conditional PDFs is that the EMST model produced an extremely narrow PDF for all mixture fraction values and times. This is in contrast to the DNS which progresses from an initially narrow conditional PDF (laminar flamelet initial condition) to a much broader PDF as mixing effects dominate, followed by a late contraction in PDF width due to a relaxation in mixing rates and an approach to equilibrium. The narrow conditional PDFs produced by the EMST model has previously been observed [45, 46], and may be attributed to the locality principle of EMST which results in the violation of independence and linearity properties [10]. The criteria for mixing to occur locally in composition space can result in the composition conforming to low dimensional manifolds, this effect is referred to as "stranding" [10] and may be the cause of the extremely narrow conditional PDFs produced with the EMST mixing model.

4.4.2. Ethylene

Conditional PDFs of temperature and OH mass fraction were obtained for the ethylene cases 1 and 3. Cases 1 and 3 were selected as they were the best and worst performing cases,
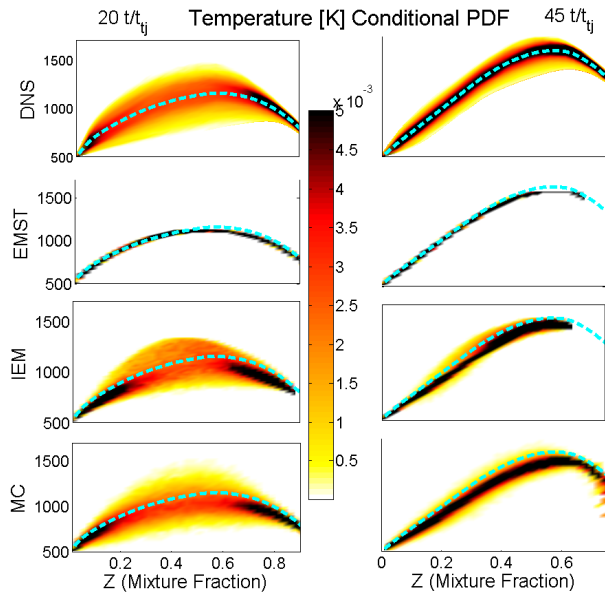
Figure 17: Probability density function of temperature conditioned on mixture fraction for case M at 20 and 45 jet times for the DNS and EMST, IEM, and MC mixing models. The cyan dashed line represents the conditional mean of the DNS for reference purposes.
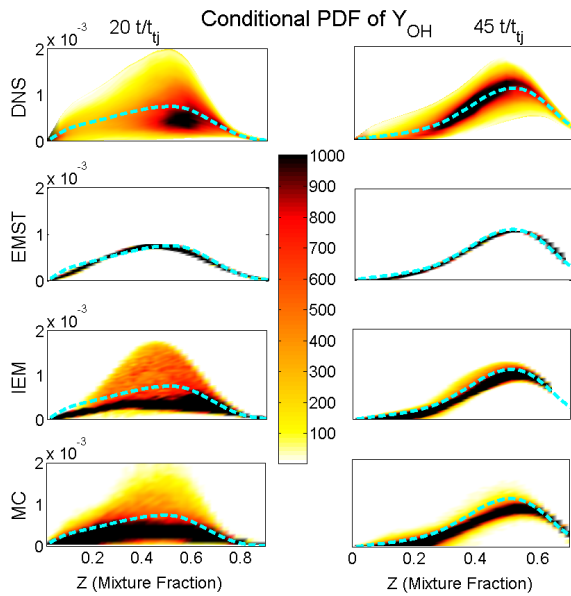
Figure 18: Probability density function of OH mass fraction conditioned on mixture fraction for case M at 20 and 45 jet times for the DNS and EMST, IEM, and MC mixing models. The cyan dashed line represents the conditional mean of the DNS for reference purposes.

26
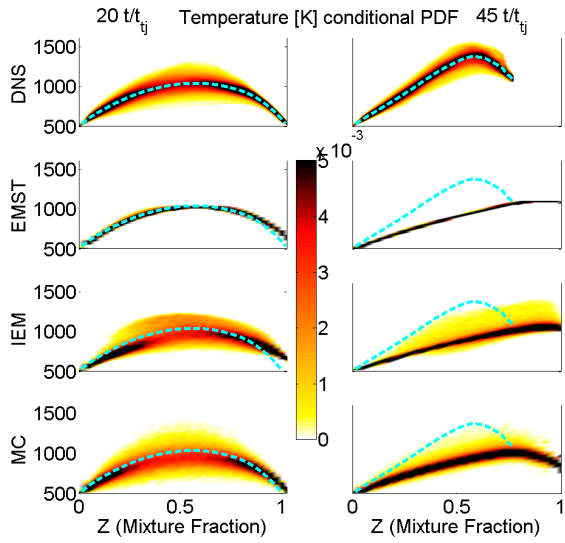
Figure 19: Probability density function of temperature conditioned on mixture fraction for case H at 20 and 45 jet times for the DNS and EMST, IEM, and MC mixing models. The cyan dashed line represents the conditional mean of the DNS for reference purposes.
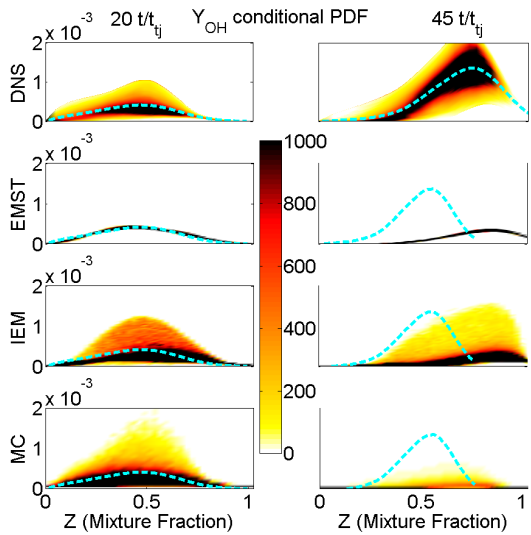
Figure 20: Probability density function of OH mass fraction conditioned on mixture fraction for case H at 20 and 45 jet times for the DNS and EMST, IEM, and MC mixing models. The cyan dashed line represents the conditional mean of the DNS for reference purposes.

27

respectively.

Figures 21 and 22 present the case 1 temperature and OH mass fraction results, respectively. This case shows bimodal behaviour, Fig. 21, where the DNS conditional PDFs show distinct burning and extinguished branches. The EMST mixing model adheres uniformly to the burning branch and produces an extremely narrow conditional PDF. The IEM and MC mixing models reproduce the bimodal behaviour with PDFs that qualitatively resemble the DNS case. However, the IEM and MC PDFs are heavily weighted to the extinguished branch, producing conditional means that significantly under-predict temperature compared to the DNS. These results are supported by Fig. 22, showing conditional PDFs of OH. The bimodal behaviour of OH in the DNS is partially reproduced by the IEM and MC model.

It is noteworthy to remark here that the global Damköhler number and, by design, most of the other parameters of the syngas case M and the ethylene cases are similar. However the results in terms of the ability of the MC and IEM models to capture the two cases are remarkably different, with the IEM and MC models providing a good agreement for case M but over-predicting extinction for case 1. It is speculated that this is due to the different nature of the extinction for these two fuels, which is related to activation energy, i.e. Zel'dovich number [47]. The ethylene flames have a much higher effective Zel'dovich number so that extinguished and burning states are clearly separated, leading to a strongly bimodal conditional PDF. In the syngas cases, extinction is more gradual and does not result in sharp changes of states, leading to a broad and mono-modal PDF. (These features are also observed experimentally [48]). Therefore, for ethylene the sensitivity to mixing is expected to be greater since a mixing event that moves a particle off the burning branch is expected to result in rapid and complete extinction. In contrast the same event in the syngas cases results in an incrementally reduced temperature, which may be sufficient to allow reignition.

Figures 23 and 24 show case 3 temperature and OH mass fraction results, respectively. Case 3 has near global extinction, which is apparent from the DNS conditional PDF. All mixing models fail to correctly predict this case. The IEM and MC models predict even more extinction compared to the DNS results, although the conditional means of temperature and
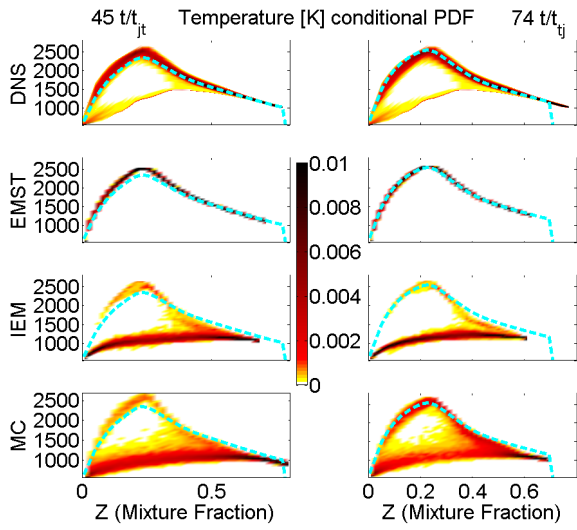
Figure 21: Probability density function of temperature conditioned on mixture fraction for case 1 at 45 and 74 jet times for the DNS and EMST, IEM, and MC mixing models. The cyan dashed line represents the conditional mean of the DNS for reference purposes.
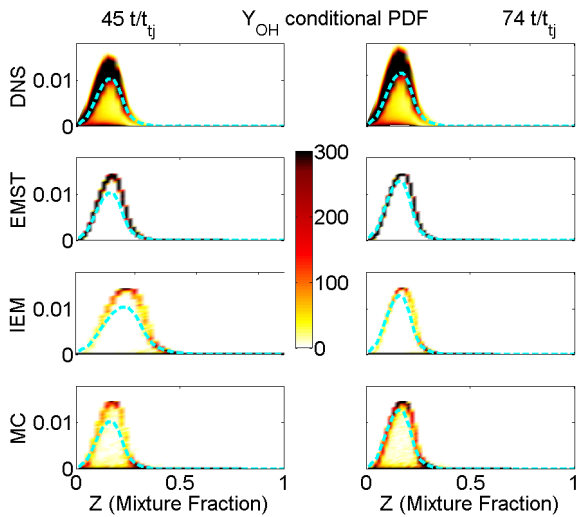
Figure 22: Probability density function of OH mass fraction conditioned on mixture fraction for case 1 at 45 and 74 jet times for the DNS and EMST, IEM, and MC mixing models. The cyan dashed line represents the conditional mean of the DNS for reference purposes.

OH mass fraction are close to the DNS. The EMST model predicts low levels of extinction and strong reignition with a narrow PDF.
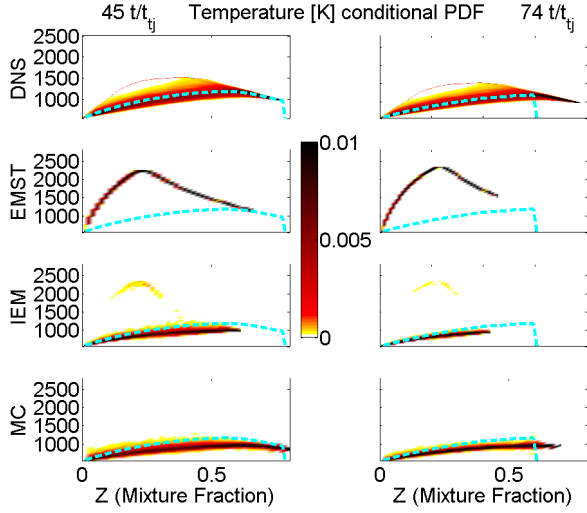
Figure 23: Probability density function of temperature conditioned on mixture fraction for case 3 at 45 and 74 jet times for the DNS and EMST, IEM, and MC mixing models. The cyan dashed line represents the conditional mean of the DNS for reference purposes.

4.5. Study of the mixing constant

A parametric study was performed for the ratio of the scalar to turbulent mixing time scales, C_ϕ, for syngas case M and ethylene case 1. Instead of extracting the mixing frequency directly from the DNS, the turbulent kinetic energy, k, and the dissipation rate of turbulent kinetic energy, ϵ, were extracted. These variables were then used to calculate the mixing frequency in the manner of a $k - \epsilon$ closure. The scalar mixing frequency was modelled as $\Omega_\phi = C_\phi \frac{\epsilon}{k}$. All other input values from the DNS were unchanged.

The implied C_ϕ value was extracted from the DNS by equating the two expressions for Ω_ϕ, i.e. $\widetilde{\chi_\phi} / \widetilde{\phi''^2}$ and $C_\phi \frac{\epsilon}{k}$. The implied, domain-averaged C_ϕ values from ethylene case 1 and syngas case M are presented in Fig. 25. The value is calculated as $C_{\phi,av} = \int_0^{y_{max}} C_\phi \widetilde{\phi''^2} \frac{\epsilon}{k} dy / \int_0^{y_{max}} \widetilde{\phi''^2} \frac{\epsilon}{k} dy$. The C_ϕ values are temporaly evolving and take a value between 1.6 and 2.1 following the transition from the initial laminar flame into a turbulent flame.
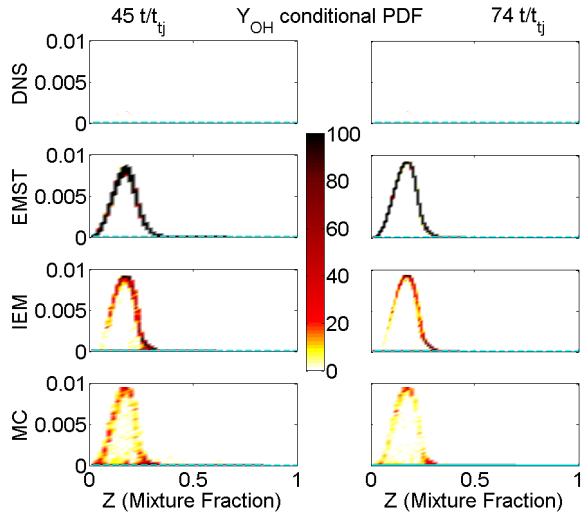
Figure 24: Probability density function of OH mass fraction conditioned on mixture fraction for case 3 at 45 and 74 jet times for the DNS and EMST, IEM, and MC mixing models. The cyan dashed line represents the conditional mean of the DNS for reference purposes.
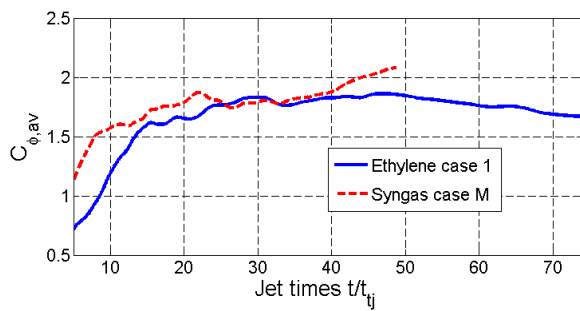
Figure 25: Domain-averaged, implied value for $C_{\phi,av}$ from ethylene case 1 (solid, blue line) and syngas case M (dashed, red line).

4.5.1. Syngas

For Case M, spatial plots for mean temperature and RMS mixture fraction profiles were produced, and are shown in Figures 26 and 27, respectively, to determine the best value for C_ϕ.

Fig. 26 shows generally good agreement between all mixing models and the DNS. The mean temperature profile is not very sensitive to C_ϕ with values from 1.6 to 3.0 producing similar results. The EMST model in particular is insensitive to the value for C_ϕ.

The mixture fraction RMS is much more sensitive to C_ϕ as displayed in Fig. 27, with increasing C_ϕ resulting in decreasing variance, as expected. Both earlier and later in the simulation the best agreement with the DNS is obtained with a value of 1.6 or 2.0 for C_ϕ. This is consistent with studies performed on shear layer turbulence [49], a previous study by Xu and Pope [18] and an *a priori* analysis of the same DNS database [22].
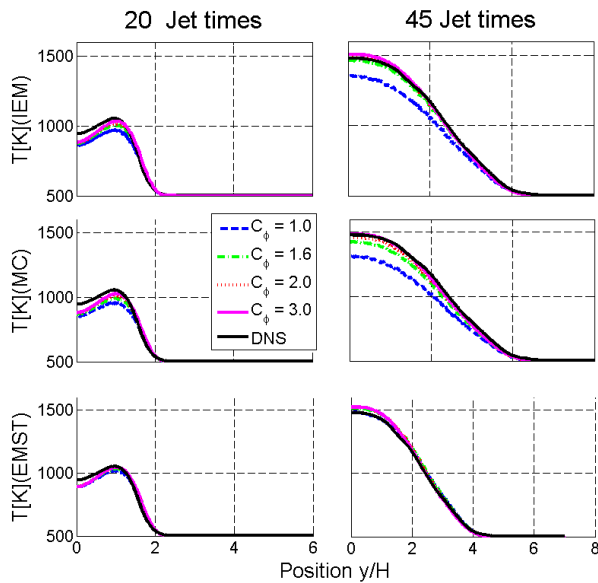
Figure 26: Mean spatial temperature profiles from parametric study of C_ϕ for syngas case M. Left column is 20 jet times, right column is 45 jet times.

4.5.2. Ethylene

The parametric variation of C_ϕ was also conducted for ethylene case 1.
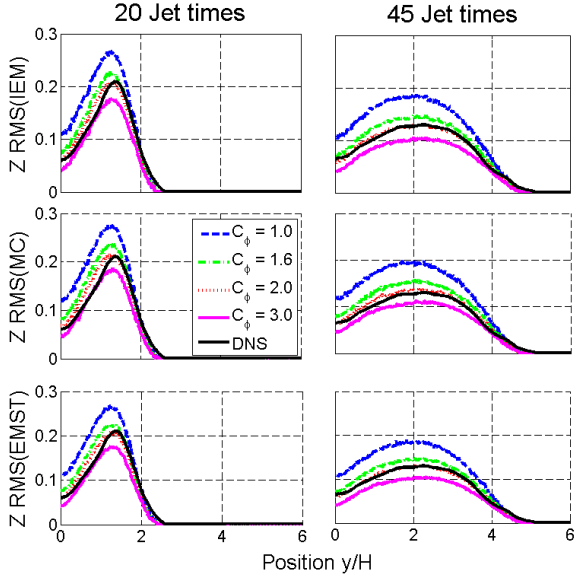
Figure 27: Spatial mixture fraction RMS profiles from parametric study of C_ϕ for syngas case M. Left column is 20 jet times, right column is 45 jet times.

Figure 28 presents the mean temperature profiles. The IEM and MC models can be made to reignite and reach good agreement with the DNS by setting C_ϕ equal to 3.0. The EMST model has the best overall performance with a value of 2.0, although there is a slight under-prediction of temperature at 74 jet times. The EMST mixing model is least sensitive to the value of C_ϕ, with values as low as 1.0 still predicting high levels of reignition. The MC model shows intermediate sensitivity, followed by the IEM model which is very sensitive to C_ϕ and is extinguished with a value of 2.0. The profiles of mixture fraction RMS, as shown in Figure 29, most closely reproduce the DNS results with a value of C_ϕ between 2.0 and 3.0. The value of 3.0 for the IEM and MC models produces a slight under-prediction of mixture fraction RMS, the value of 2.0 for the EMST model produces a slight over-prediction.

All of the mixing models can be made to reproduce the extinction and reignition in case 1 by choosing a suitable value for C_ϕ. Figure 30 reveals the qualitatively correct evolution of the temperature field for all mixing models. This is in contrast to the extinguished results for the IEM and MC models obtained by extracting the mixing frequency based on the Bilger mixture fraction directly from the DNS, see Fig. 13.
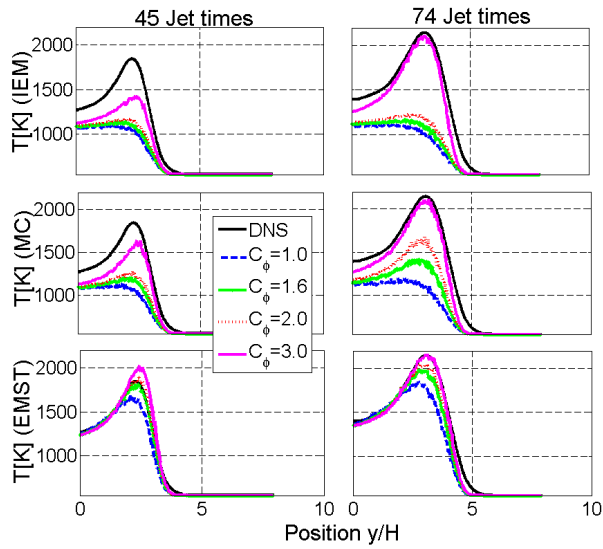
Figure 28: Mean spatial temperature profiles from parametric study of C_ϕ for ethylene case 1. Left column is 45 jet times, right column is 74 jet times.
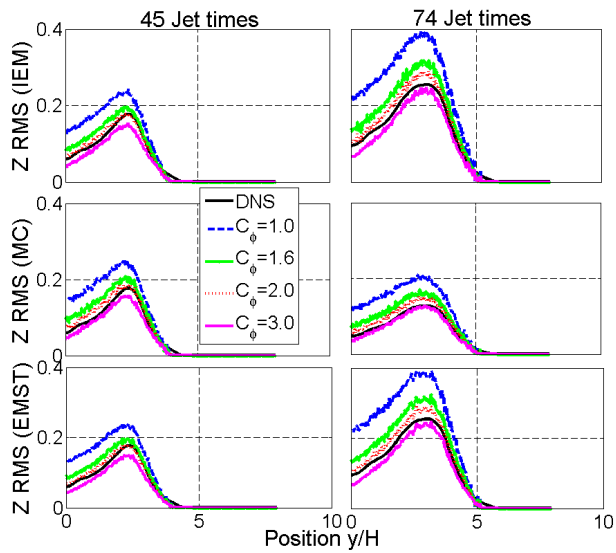
Figure 29: Spatial mixture fraction RMS profiles from parametric study of C_ϕ for ethylene case 1. Left column is 45 jet times, right column is 74 jet times.

34
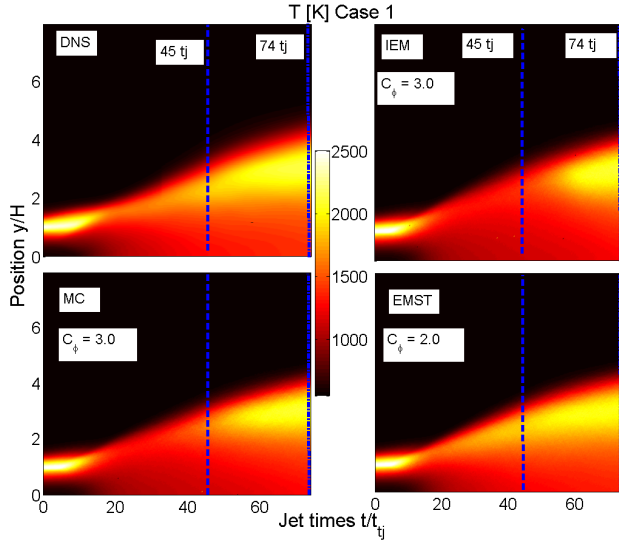
Figure 30: Extinction and reignition for case 1 using the best value for C_ϕ for each mixing model. The domain coloured by mean temperature shows the one-dimensional spatial profile's progression over time.

4.6. Discussion

The results indicate that both the degree of extinction and the fuel properties impact the performance of the models. For a given fuel, increasing the level of extinction makes it more difficult to capture reignition. However, the fuel-related flame characteristics are also important. As described in Ref. [27], ethylene and syngas have contrasting flame properties. Syngas produces a broader flame with a lower extinction temperature compared to ethylene, making syngas more likely to reignite. Fuel-related characteristics also determine which reignition modes are dominant. We consider flame-flame interactions (FFI) and the propagation of edge flames to be the two primary reignition modes [27]. FFI is a nonpremixed mode that involves the turbulent transport of burning stoichiometric regions to non-burning stoichiometric regions to trigger reignition. Reignition by FFI is more likely for a flame with a broad reaction zone as flammable regions are more common and therefore more likely to interact. Moreover, this mode is driven fundamentally by turbulent mixing, which is a process that is certainly represented by the mixing models (particularly the pair-wise exchange models). In contrast, edge flame propagation involves a premixed edge flame propagating along the stoichiometric surface to heal extinguished regions. As the premixed flame im-

35

poses its own length and timescales, this mechanism is arguably not driven by turbulent mixing, and therefore it is arguably not represented by the mixing models. Inspection of the ethylene DNS indicates that edge flame propagation is an important mechanism [27], while in the syngas case FFI was more prominent [22]. This may explain why the reignition of the broader syngas flame is predicted relatively better compared to the thinner ethylene flame.

For a flame with a broad reaction zone, the results from syngas cases L and M show that there is limited sensitivity to the mixing model selected. The results from ethylene cases 1 and 2 show that for the thinner flame the choice of mixing model becomes very important with only the EMST model being capable of capturing reignition without arbitrarily adjusting the mixing constant. This result is consistent with the study by Subramaniam and Pope [39]. In that study a numerical experiment was conducted consisting of repeated parallel slabs of fuel and oxidizer, designed to mimic the structure of a turbulent non-premixed flame-brush. A parametric variation of reaction zone thickness and Damköhler number was performed and it was found that both the IEM and EMST models were successful in predicting extinction and burning solutions only for the case of a broad reaction zone. In the moderate and thin reaction zone cases the IEM model consistently over predicted extinction, whereas the EMST model did not.

In the present study, the IEM and MC models produce broadly similar spatial and conditional results. This is consistent with early mixing model comparative studies [50, 51]. Nooren *et al.* [50] compared the IEM and MC models for a natural gas nonpremixed flame using a C_ϕ value of 2.0 for both models. Mean and RMS temperature spatial profiles were generally well-predicted by both models. Wouters *et al.* [51] conducted a numerical experiment in a gas-phase jet configuration and found generally good agreement with the spatial evolution of mixture fraction PDFs.

In contrast, major differences between IEM and MC models were observed in the mixing model comparison study for the Delft III burner by Merci *et al.* [45]. In this study the IEM, MC, and EMST models were compared. C_ϕ was adjusted to optimize the solution for each mixing model. While the MC model could reproduce the correct attached flame structure with a C_ϕ value of 3.0, no burning solution was possible with the IEM model.

The resistance to extinction of the EMST mixing model observed in this study is consistent with previous numerical and experimental comparative studies of mixing models [39, 45, 46, 52]. In a study of Sydney Flame burners HM1-3 by Merci *et al.* [46], it was found that for the most turbulent case, HM3, that only the EMST model was able to correctly produce a burning solution.

The tendency of the EMST mixing model to adhere to the burning solution is favourable for the flames in this study with high levels of local extinction (see figures 13 and 14) and in Refs. [39, 45, 46]. However, the results from ethylene case 3 reveal that this can lead to extreme over-prediction of reignition. The narrow, mono-modal shape of the EMST conditional PDFs are presumably the cause. The under-prediction of conditional scalar RMS was also observed in Refs. [45, 46]. However, the EMST model has been shown in another study to correctly produce broader, bi-modal conditional PDFs [52].

The study of the mixing constant C_ϕ in syngas case M and ethylene case 1 suggests that the best value of C_ϕ and the sensitivity to this parameter are dependent upon the mixing model and the simulation case. For case M, all mixing models were qualitatively correct over a large range of C_ϕ values. For case 1, the IEM and MC models were much more sensitive to C_ϕ compared to the EMST model. This is consistent with previous studies of flames with high levels of extinction [45, 52]. Those studies demonstrated the need to "tune" the IEM and MC models via the C_ϕ constant in order to obtain correct results, whereas the EMST model performs well with C_ϕ in the range of 1.5 to 2.0, for both case M and case 1.

5. Conclusions

An evaluation of the IEM, MC and EMST mixing models was performed in the context of a RANS-based C-TPDF method. The C-TPDF model was compared with DNS of turbulent non-premixed jet flames with either syngas or ethylene as the fuel. In contrast to previous studies, in the present work the mean mixing frequency, mean velocity, and turbulent diffusion coefficient were taken directly from a DNS database, enabling the elimination of several possible sources of modelling error. In addition, numerical parameters were chosen

to eliminate numerical inaccuracy as a source of error. Thus, the present results offer direct evaluations of the consequences of errors in mixing and turbulent transport models.

In terms of predictions of mean quantities, the following remarks may be made pertaining to the cases where the mixing frequency was determined from gradients and fluctuations of mixture fraction. For the syngas case, all three mixing models were found to perform well in cases without extensive extinction (L and M). However, they under-predicted reignition in a case with more extinction (H), with EMST performing slightly better than the IEM and MC models. For the ethylene cases, differences between the models became more noticeable, with EMST performing better in higher Damköhler number cases that locally extinguished but reignited (cases 1 and 2), and with IEM and MC significantly over-predicting levels of extinction. In contrast, EMST incorrectly predicted a fully burning flame in a case that is nearly fully extinguished (case 3), while IEM and MC more closely predict the nearly extinguished state. Thus, the predictions were shown to be fuel dependent. It is hypothesized that the greater sensitivity to the mixing model observed for ethylene can be traced to a relatively higher effective Zel'dovich number which causes sharp transitions between burning and extinguished states.

When conditional statistics were examined, EMST was shown to always significantly underestimate conditional variances. While the MC and IEM models could not predict the global mean structure, they did offer qualitative improvements in features of the scalar conditional PDFs. They correctly predicted a broad and mono-modal PDFs in the syngas cases and bi-modal PDFs in the ethylene cases, whereas the EMST model always predicted a narrow, mono-modal PDF.

To provide guidance on the selection of the mixing constant, simulations were performed constructing the mixing frequency from the DNS values of k and ϵ and an assumed mixing constant. These tests revealed C_ϕ in the range of 1.6 to 2.0 provided the best results for syngas case M, in line with recommendations from other studies. For ethylene case 1, the EMST model performed best with a value of 2.0, but the MC and IEM models required a value of 3.0.

Overall, the results demonstrate that if all the sub-models used are accurate (turbu-

lence, mixing frequency, chemistry, etc), that the C-TPDF method can provide excellent predictions even in challenging circumstances. They also demonstrate limitations of the method, at least for its implementation in RANS, as some cases cannot be predicted by any of the tested models despite all required information being provided directly from DNS. The authors speculate that LES may be necessary to make further improvements.

In terms of recommendations for model selection, overall the results suggest that for flames without strong extinction, there is little to distinguish between the models which implies that the simpler models should suffice. For cases with extensive extinction, EMST is recommended despite its underestimating conditional fluctuations, as the other models significantly over-predict extinction, which practically may result in no prediction at all as the flame may blow off. A relatively lower sensitivity of the results to the value of C_ϕ is another distinct advantage. However, it should be noted that the EMST model may fail to reproduce global extinction where appropriate.

Future directions of this research will include similar assessments for other scenarios including premixed flames [53] and lifted flames [54, 55].

6. Acknowledgements

References

[1] S. B. Pope, Prog. Energ. Combust. Sci. 11 (1985) 119–192.

[2] S. B. Pope, Phys. Fluids 23 (2011) 011301.

[3] R. W. Bilger, S. B. Pope, K. N. C. Bray, J. F. Driscoll, Proc. Combust. Inst. 30 (2) (2005) 21–42.

[4] D. Haworth, Prog. Energ. Combust. Sci. 36 (2010) 168–259.

[5] R. R. Cao, S. B. Pope, Combust. Flame 143 (2005) 450–470.

[6] S. Mitarai, J. J. Riley, G. Kosály, Phys. Fluids 17 (4) (2005) 047101.

[7] J. Villermaux, J. C. Devillon, in: P. 2nd Int. Symp. on Chem. Reaction Eng. (1972) 1–13.

[8] R. L. Curl, AIChE J. 9 (1963) 175–181.

[9] J. Janicka, W. Kolbe, W. Kollmann, J. Non-Equil. Thermody. 4 (1979) 47–66.

[10] S. Subramaniam, S. B. Pope, Proc. Combust. Inst. 115 (1998) 487–514.

[11] V. Raman, H. Pitsch, R. Fox, Combust. Flame 143 (2005) 56–78.

[12] S. James, J. Zhu, M. S. Anand, Proc. Combust. Inst. 31 (2) (2007) 1737–1745.

[13] W. P. Jones, S. Navarro-Martinez, Combust. Flame 150 (3) (2007) 170–187.

[14] R. P. Lindstedt, S. A. Louloudi, E. M. Vaos, Proc. Combust. Inst. 28 (2000) 149 – 156.

[15] A. R. Masri, R. R. Cao, S. B. Pope, G. M. Goldin, Combust. Theor. Model. 8 (2003) 1–22.

[16] R. P. Lindstedt, S. A. Louloudi, Proc. Combust. Inst. 29 (2) (2002) 2147–2154.

[17] Q. Tang, J. Xu, S. B. Pope, Proc. Combust. Inst. 28 (2000) 133 – 139.

[18] J. Xu, S. B. Pope, Combust. Flame 123 (3) (2000) 281 – 307.

[19] B. Merci, B. Naud, D. Roekaerts, Flow Turbul. Combust. 74 (3) (2005) 239–272.

[20] S. B. Pope, *Mixing model performance in the calculation of nonpremixed piloted jet flames,* in Proceedings of the Sixth International Workshop on Measurement and Computation of Turbulent Nonpremixed Flames Combustion Institute, Sapporo (2002).

[21] Y. Yang, H. Wang, S. B. Pope, J. H. Chen, Proc. Combust. Inst. 34 (2013) 1241–1249.

[22] E. R. Hawkes, R. Sankaran, J. C. Sutherland, J. H. Chen, Proc. Combust. Inst. 31 (2007) 1633–1640.

[23] E. R. Hawkes, R. Sankaran, J. H. Chen, S. A. Kaiser, J. H. Frank, Proc. Combust. Inst. 32 (2009) 1455–1463.

[24] B. A. Sen, E. R. Hawkes, S. Menon, Combust. Flame 157 (2010) 566–578.

[25] N. Punati, J. C. Sutherland, A. R. Kerstein, E. R. Hawkes, J. H. Chen, Proc. Combust. Inst. 33 (2011) 1515–1522.

[26] D. O. Lignell, J. H. Chen, H. A. Schmutz, Combust. Flame 158 (5) (2011) 949 – 963.

[27] D. O. Lignell, D. S. Rappleye, Combust. Flame 159 (2012) 2930 – 2943.

[28] R. R. Cao, H. Wang, S. B. Pope, Proc. Combust. Inst. 31 (2007) 1543–1550.

[29] S. James, J. Zhu, M. S. Anand, Proc. Combust. Inst. 31 (2) (2007) 1737 – 1745.

[30] M. R. H. Sheikhi, T. G. Drozda, P. Givi, F. A. Jaberi, S. B. Pope, Proc. Combust. Inst. 30 (2005) 549 – 556.

[31] S. B. Pope, Turbulent Flows, Cambridge University Press, 1st edition, 2000.

[32] C. Dopazo, E. E. O'Brien, Acta. Astronaut. 1 (1974) 1239–1266.

[33] A. R. Masri, S. Subramaniam, S. B. Pope, Proc. Combust. Inst. 26 (1996) 49–57.

[34] S. Viswanathan, H. Wang, S. B. Pope, J. of Comput. Phys. 230 (17) (2011) 69166957.

[35] C. A. Kennedy, M. H. Carpenter, R. M. Lewis, Appl. Numer. Math. 35 (3) (2000) 177–219.

[36] G. Strang, SIAM J. Numer. Anal. 5 (3) (1968) 506–517.

[37] H. Wang, P. P. Popov, S. B. Pope, J. Comput. Phys. 229 (5) (2010) 1852 1878.

[38] Z. Ren, S. Subramaniam, S. B. Pope, *Implementation of the EMST mixing model*, http://tcg.mae.cornell.edu/emst (2013).

[39] S. Subramaniam, S. B. Pope, Combust. Flame 117 (4) (1999) 732 – 754.

[40] A. Y. Klimenko, S. B. Pope, Physics of Fluids (1994-present) 15 (2003).

[41] M. Cleary, A. Klimenko, Flow, Turbulence and Combustion 82 (2009) 477–491.

[42] S. B. Pope, Phys. Fluids 25 (2013) 110803.

[43] K. R. Sreenivasan, Flow Turbul. Combust. 72 (2) (2004) 115–131.

[44] P. Sripakagorn, G. Kosály, J. J. Riley, Combust. Flame 136 (3) (2004) 351–363.

[45] B. Merci, D. Roekaerts, B. Naud, Combust. Flame 144 (3) (2006) 476–493.

[46] B. Merci, D. Roekaerts, B. Naud, S. B. Pope, Combust. Flame 146 (2006) 109–130.

[47] P. Sripakagorn, S. Mitarai, G. Kosály, H. Pitsch, J. Fluid Mech. 518 (2004) 231–259.

[48] A. R. Masri, R. W. Bilger, Combust. Flame 81 (1990) 260–276.

[49] C. Béguier, I. Dekeyser, B. E. Launder, Phys. Fluids 21 (3) (1978) 307.

[50] P. A. Nooren, H. A. Wouters, T. W. J. Peeters, D. Roekaerts, U. Maas, D. Schmidt, Combust. Theor. Model. (1997) 37–41.

[51] H. A. Wouters, P. A. Nooren, T. W. J. Peeters, D. Roekaerts, Int. J. Heat Fluid Fl. 19 (1998) 201–207.

[52] R. R. Cao, H. Wang, S. B. Pope, Proc. Combust. Inst. 31 (2007) 1543–1550.

[53] E. R. Hawkes, O. Chatakonda, H. Kolla, A. R. Kerstein, J. H. Chen, Combust. Flame 159 (8) (2012) 2690–2703.

[54] C. S. Yoo, R. Sankaran, J. H. Chen, J. Fluid Mech. 640 (2009) 453.

[55] C. S. Yoo, E. S. Richardson, R. Sankaran, J. H. Chen, Proc. Combust. Inst. 33 (2011) 1619–1627.